CHAPTER 2

MATHEMATICAL MODEL OF BIPOLAR PLATE FOR (PEMFC)

CHAPTER (2)
MATHEMATICAL MODEL OF BIPOLAR PLATE FOR (PEMFC)

2.1 INTRODUCTION

Bipolar plates (BPPs) being one of the most important components in PEMFC stacks must perform a number of functions simultaneously in order to achieve good stack performance and lifetime. BPPs supply the reactant gases through the flow channels to the electrodes and serve the purpose of electronically connecting one cell to another in the electrochemical cell stack. These plates also provide structural support for the thin and mechanically weak MEAs and the means to facilitate water management within the cell, in the absence of dedicated cooling plates. Therefore, the optimal design must be sought for the BPPs because the above functions have conflicting requirements on the BPP design.

The Computational Fluid Dynamic (CFD) is a very useful tool to simulate hydrogen and oxygen gases flow channels configurations, reducing the costs of bipolar plates' production and optimizing mass transport [46-48].

BPPs have been studied by using commercial computational fluid dynamics (CFD) tool (COMSOL). The incompressible Navier-Stokes equations in the flow channels and the Brinkman equations for the porous gas diffusion layers (GDLs), using the free and porous media flow interface has been solved by COMSOL to define the best design. The obtained results give a designer the good idea on which design parameters would be optimal to get the best PEMFC performance.

2.2 MATHEMATICAL MODEL

The performance of proton exchange membrane fuel cell (PEMFC) is directly proportional to the flow channel design on bipolar plates. The cell voltage and the cell power density can be increased by varying the channel size geometry types or arrangement. The objective from this thesis is to present new flow channel patterns serpentine with square end two, three and six passes and serpentine with circular end two, three and six passes and study them by using commercial computational fluid dynamics (CFD) tool (COMSOL). The flow is assumed to be steady, laminar, and incompressible in both flow channels and the gas diffusion layer, the fuel cell is assumed to operate isothermally. The momentum transport in a flow channel is governed by Navier–Stokes Eq. (2.1); the mass transport in both regions is governed by the continuity Eq. (2.2).and the momentum transport in the porous gas diffusion layer is governed by Brinkman's Eq. (2.3).

Flow in the free channel is described by the Navier-Stokes equations:

$$\rho ux\nabla .u = \nabla[-PI + \mu(\nabla u + \nabla u^T)] \tag{2.1}$$

Where μ denotes the fluid Dynamic viscosity, (Pa.s), u the velocity vector in the open channel (m s^{-1}), ρ the density of the fluid (kg m^{-3}), p pressure (Pa) and I identity matrix.

The continuity equation:

$$\nabla .u = 0 \tag{2.2}$$

In the porous domain, flow is described by the Brinkman equations according:

$$(\frac{\mu}{k})u = \nabla[-PI + (\frac{1}{\varepsilon})\mu(\nabla u + \nabla u^T)] \tag{2.3}$$

Where k denotes the permeability of the porous medium (m^2), and ε is the porosity of the gas diffusion layer.

Simultaneously the two equations will be coupled and implemented to (COMSOL multiphysics 4.2.a) to solve both equation systems for different variable names of the velocity and pressure,

The main boundary conditions which have been created for each flow pattern are as following:

In the inlet boundary, the fluid velocity was given. In the outlet boundary, the outlet pressure was set to atmospheric pressure. A 'no-slip' condition was used for all of the wall boundaries. Finally, the Navier–Stokes Eq. (2.1) for the flow in the channel and Brinkman's Eq. (2.3) for the flow in porous gas diffusion layer are coupled along the interface between the GDL and channel through a 'continuity boundary' condition given as bellows:

$$u_{NS} = u_{Brinkman} \tag{2.4}$$

$$P_{NS} = P_{Brinkman} \tag{2.5}$$

All the boundary conditions for the Navier-Stokes equations (bipolar plate domain) are:

$$u_n = u_0 \qquad \text{Inlet} \tag{2.6}$$

$$u = 0 \qquad \text{No slip} \qquad (2.7)$$

$$u_t = 0 \qquad \text{Outlet} \qquad (2.8)$$

$$p = 0 \qquad \text{Outlet} \qquad (2.9)$$

$$p = p_1 \qquad \text{N-S-Brinkman boundary} \qquad (2.10)$$

Where the pressure at the outlet is set to zero, for use as a reference. The expression for the pressure at the boundary between the channel and the porous domain states that the pressure is continuous across this interface.

The corresponding boundary conditions for the Brinkman equations (GDL domain) are:

$$u = 0 \qquad \text{No slip.} \qquad (2.11)$$

$$u = u_1 \qquad \text{N-S-Brinkman boundary} \qquad (2.12)$$

These conditions imply that the components of the velocity vector are continuous over the interface between the free channel and the porous domain.

The input data in the model is given in table (2.1) input data:

Table 2.1 input data

Name	values	unit
ρ for GDL	2800	Kg/m^3
μ for GDL	$2.46x10^{-5}$	Pa.s
k for GDL	$1.18x10^{-11}$	m^2
ε for GDL	0.4	-
u_0	0.2	m/s

2.3 MESH REFINEMENT STUDY

To study the mesh and discover the optimum size for the mesh element, different types of mesh have been studied. Every type has maximum element size, minimum element size,

maximum element growth rate, resolution of curvature, resolution of narrow regions and also change the number of element every time as shown in table (2.2).

Table 2.2 Types of mesh.

types	maximum element size (m)	minimum element size (m)	maximum element growth rate	resolution of curvature	resolution of narrow regions	the number of element every type
Coarse	0.021	0.00392	1.6	0.7	0.4	29652
Normal	0.014	0.00252	1.5	0.6	0.5	45923
Fine	0.0112	0.0014	1.45	0.5	0.6	75215
Finer	0.0077	5.6E-4	1.4	0.4	0.7	164201
Extra fine	0.0049	2.1E-4	1.35	0.3	0.85	399234
Extremely fine	0.0040	1.1E-4	1.30	0.2	0.9	581004

The channels are meshed using free tetrahedral type of meshing that uses hexagonal elements, every type from the table was used in our model and the pressure drop exchanged for the constant effective area as shown in figure (2.1).

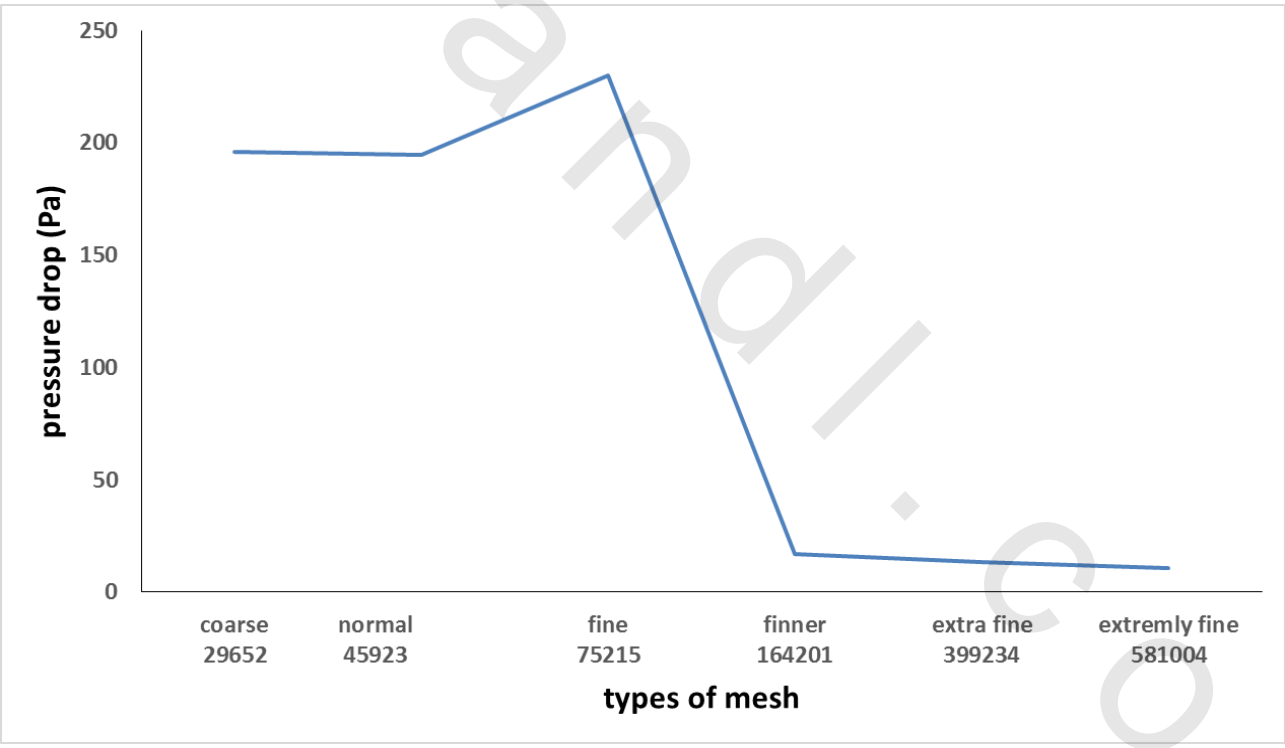

Figure 2.1 The relation between pressure drop and mesh types.

Figure (2.1) showed that before finer type the pressure drop is not stable but after it, the pressure drop is approximately stable, the optimum mesh type depends on stability and the model time to solve. This time depends on the number of elements of mesh. Time increases when number of elements increases. As a result the optimum type of mesh is the finer type.

2.4 VERIFICATION OF THE NUMERICAL MODEL

In order to verify the model presented a mathematical model data of pressure drop curve reported by Alex Bates et al. [49] were reproduced numerically using the same operating conditions, material properties and dimensions.

From figure (2.2) our calculated results for pressure drop was 3376 Pa while figure (2.3) (published data) showed pressure drop was 3507 Pa.

The results presented from the present mathematical model carried out by COMSOL 4.2 showed a good agreement with those in published paper using MUMPS (MUltifrontal Massively Parallel sparse direct Solver) demonstrating that the maximum division between our results compared by published one was 4% only.

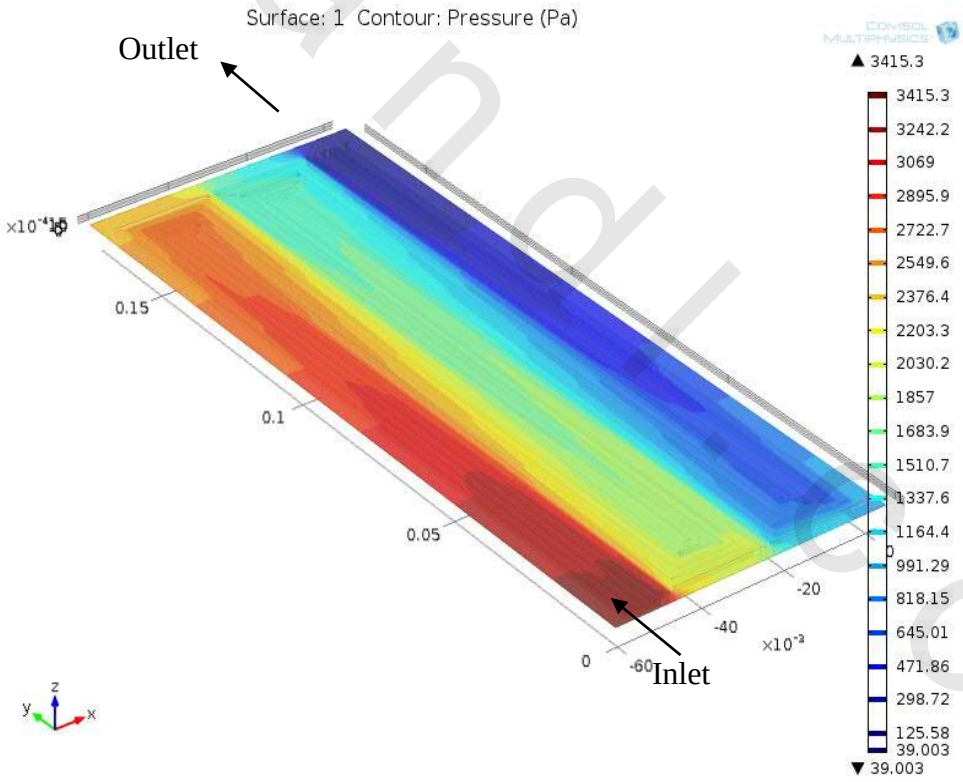

Figure 2.2 Pressure variation along channels for the present mathematical model.

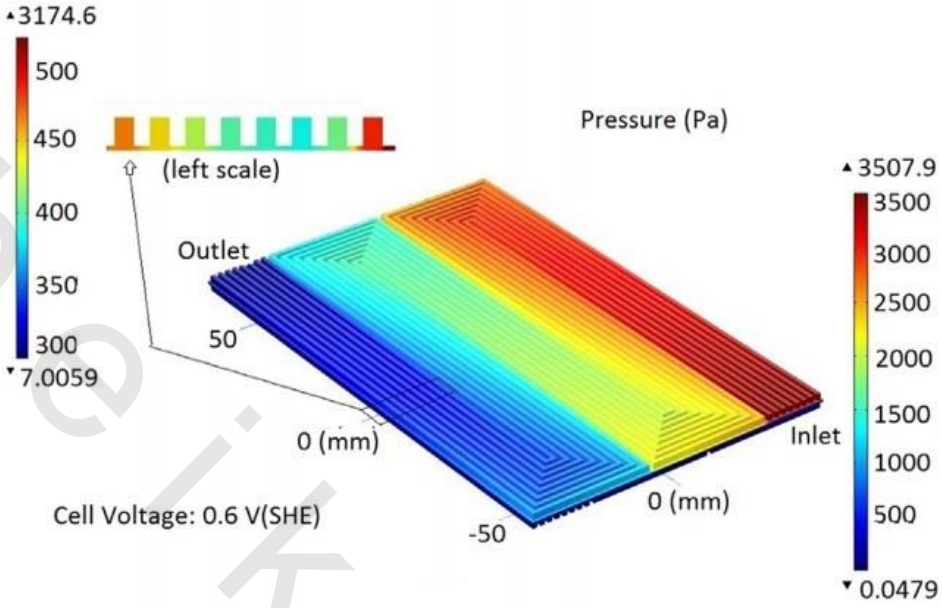

Figure 2.3 Pressure variation along channels [49].

2.5 BIPOLAR PLATE DESIGNS

2.5.1 Parallel or straight bipolar plate

This design used for air only as shown in figure (2.4)

Figure 2.4 3D designs with 1 mm width, 1 mm depth and 1 mm rip for parallel or straight bipolar plate

2.5.2 Header serpentine

This designs used for air and H_2 as shown in figure (2.5)

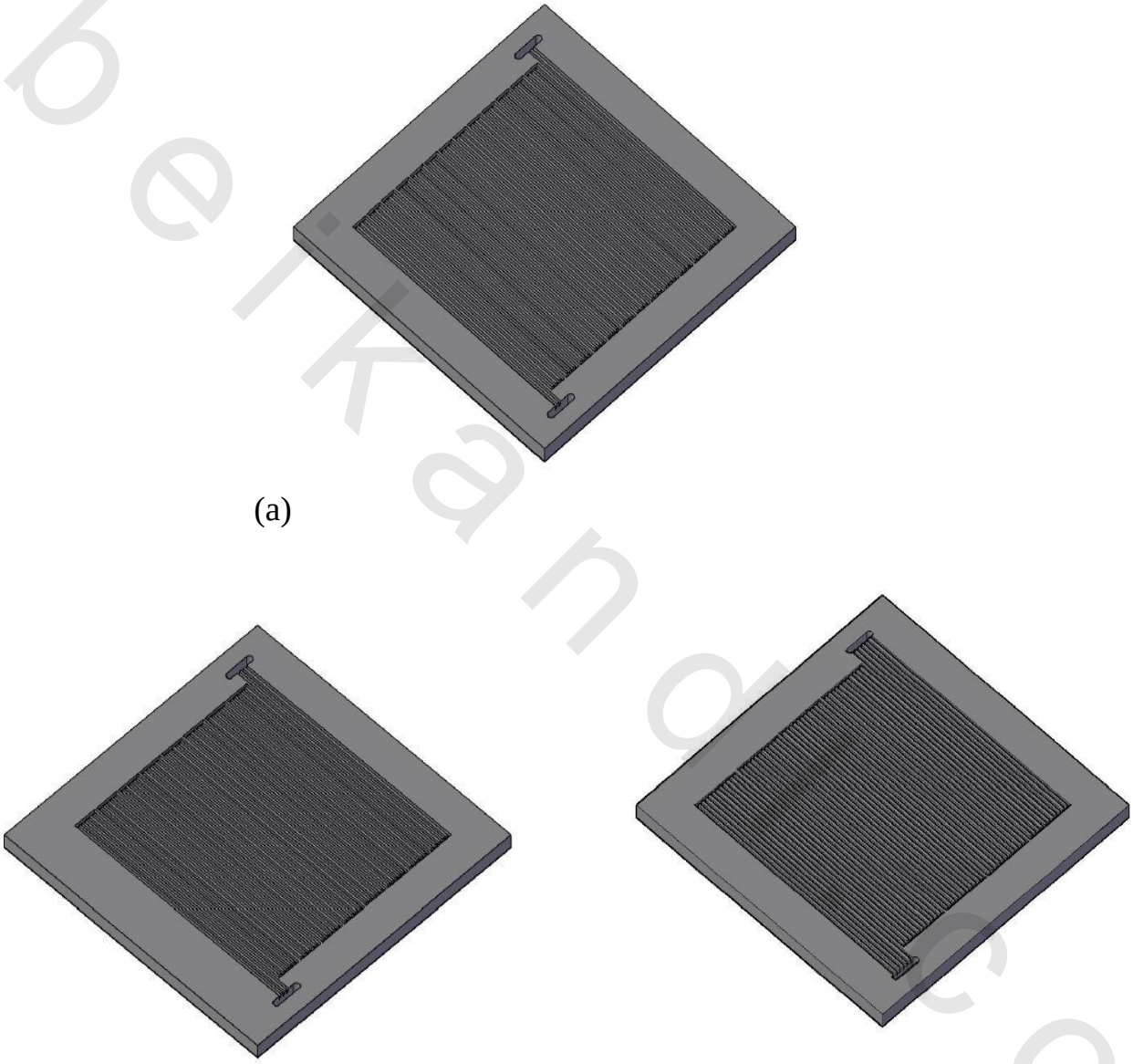

(a)

(b) (c)

Figure 2.5 3D designs with 1 mm width, 1 mm depth and 1 mm rip (a) dual channel header serpentine, (b) triple channel header serpentine, (c) sixth channel header serpentine.

2.5.3 Serpentine flow channels with square bend

This designs used for air and H_2 as shown in figure (2.6)

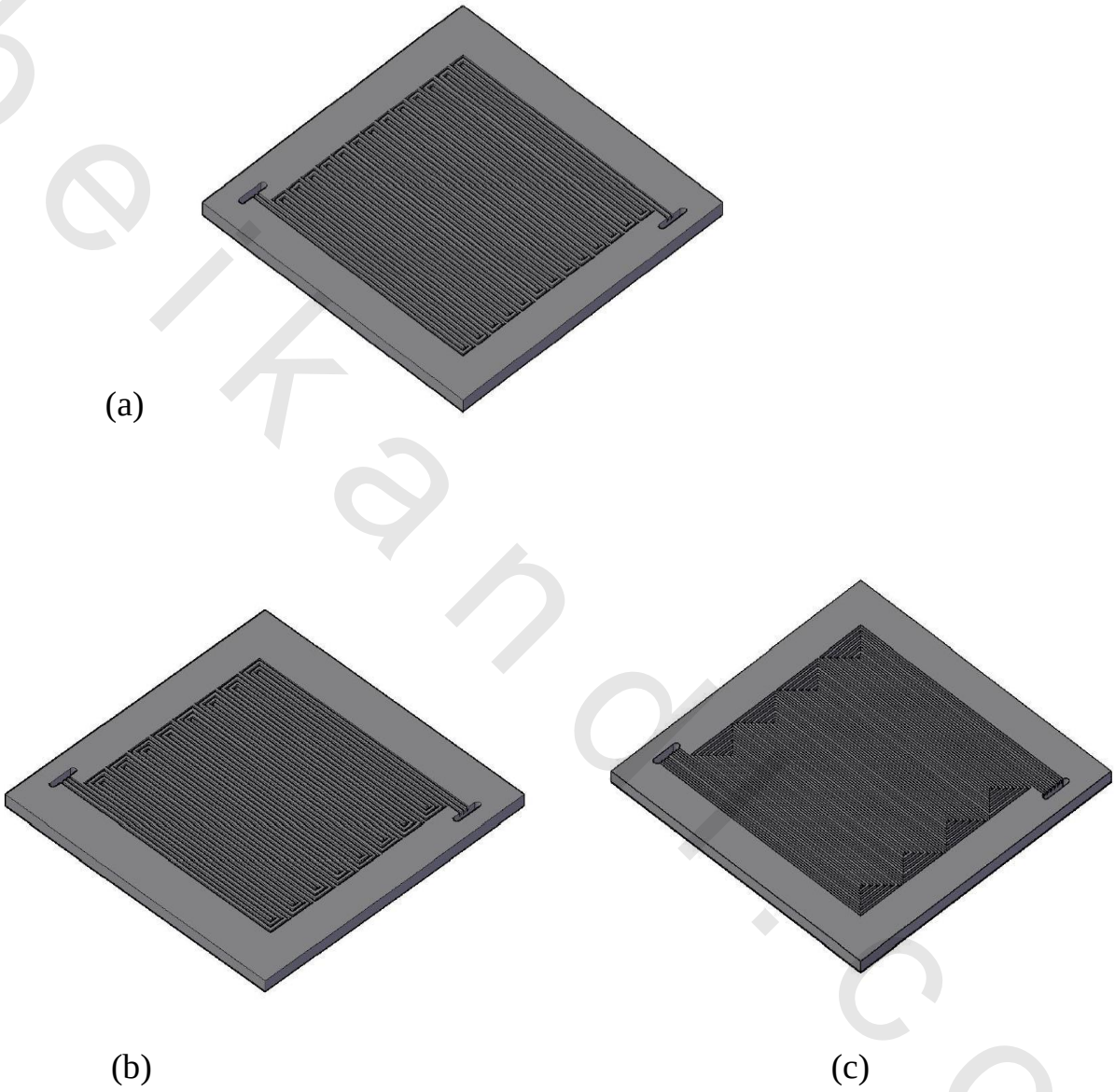

(a)

(b) (c)

Figure 2.6 3D designs with 1 mm width, 1 mm depth and 1 mm rip (a) dual serpentine flow channels with square bend, (b) triple serpentine flow channels with square bend, (c)sixth serpentine flow channels with square bend.

2.5.4 Serpentine flow channels with curvilinear bend

This designs used for air and H_2 as shown in figure (2.7)

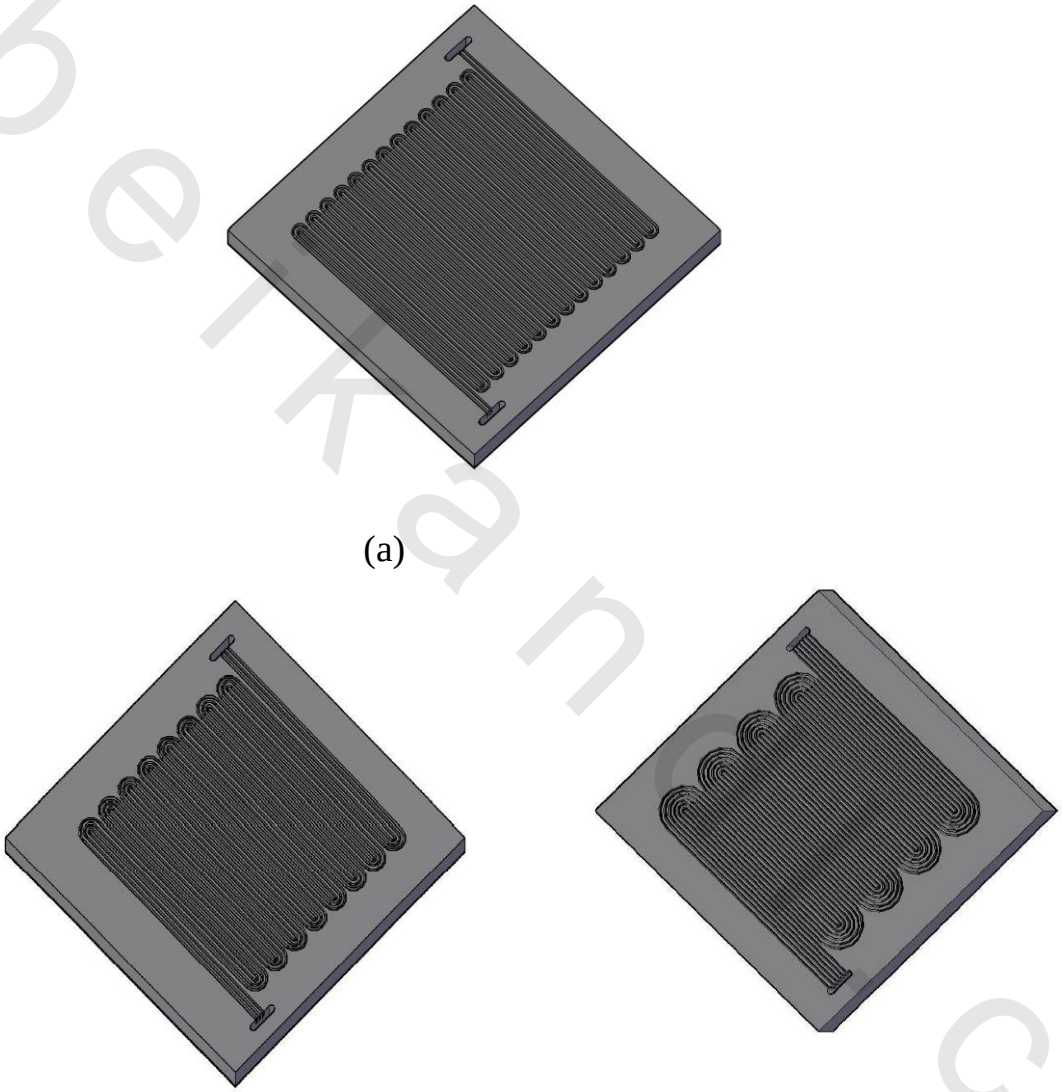

(a)

(b) (c)

Figure 2.7 3D designs with 1 mm width, 1 mm depth and 1 mm rip (a) dual serpentine flow channels with curvilinear bend, (b) triple serpentine flow channels with curvilinear bend, (c)sixth serpentine flow channels with curvilinear bend.

2.5.5 Spiral design

This designs used for air and H_2 as shown in figure (2.8)

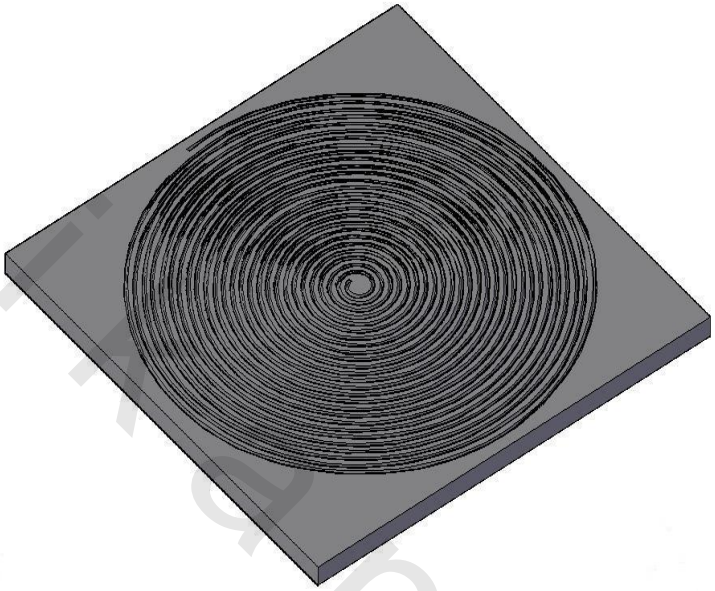

Figure 2.8 3D spiral design with 1 mm width, 1 mm depth and 1 mm rip.

All the pervious designs were physically modeled with comsol multiphysics 4.2 and by using server FUJITUS Intel (R) xeon (R) cpu E5630 @2.53 GHZ, 2.53 GHZ (2 processors) ,RAM 64 GB.

Next chapter describes and investigates the model results of bipolar plates in PEMFC.